# Highly efficient red electrophosphorescent device incorporating a bipolar triphenylamine/bisphenylsulfonyl-substituted fluorene hybrid as the host

**Fang-Ming Hsu,[a] Chen-Han Chien,[a] Ya-Jou Hsieh,[a] Chen-Hao Wu,[a] Ching-Fong Shu,*[a] Shun-Wei Liu[b] and Chin-Ti Chen*[b]**

***Received 27th May 2009, Accepted 19th August 2009***
***First published as an Advance Article on the web 15th September 2009***
**DOI: 10.1039/b910292b**



We have fabricated highly efficient red phosphorescent organic light-emitting diodes (PHOLEDs) incorporating a bipolar host material, 2,7-bis(phenylsulfonyl)-9-[4-(*N*,*N*-diphenylamino)phenyl]-9-phenylfluorene (**SAF**), doped with 7 wt% tris(1-phenylisoquinolinolato-$C^2$,*N*)iridium(III) [Ir(piq)$_3$]. Attaching the electron-donating (*p*-type) triphenylamine group onto the electron-accepting (*n*-type) 2,7-bis(phenylsulfonyl)fluorene segment (through the C9 position of the fluorene unit) imparts **SAF** with good morphological stability, high triplet energy gap ($E_T$), bipolar transporting ability, and matching energy levels with adjacent carrier-transporting layers. Consequently, the **SAF**-based red-PHOLED exhibited a very low turn-on voltage (2.4 V) and high electroluminescence efficiencies of 15.8% and 22.0 lm W$^{-1}$, superior to those of the corresponding device incorporating a conventional host material, 4,4′-*N*,*N*′-dicarbazolbiphenyl (**CBP**; 3.2 V, 8.5%, and 8.4 lm W$^{-1}$, respectively). At a practical brightness of 1000 cd m$^{-2}$, the efficiencies of the **SAF**-based red-PHOLED remained high (13.1%, 14.4 lm W$^{-1}$).

## Introduction

Phosphorescent organic light-emitting diodes (PHOLEDs) have attracted much attention because they can, in theory, approach 100% internal quantum efficiency by harvesting both singlet and triplet excitons.[1–10] In these PHOLEDs, the triplet emitters are usually doped into a host material to reduce the self-quenching associated with the relatively long excited state lifetimes of triplet emitters and triplet–triplet annihilation.[11] Thus, the development of effective hosts and phosphors is equally important for the fabrication of highly efficient PHOLEDs. Being one of the primary colors, the efficient emission of red light from OLEDs is critical for applications in full-color displays and solid state lighting.[12–16] Realizing efficient red-PHOLEDs, however, remains a great challenge because of the lack of suitable host materials. Although the carbazole derivative 4,4′-*N*,*N*′-dicarbazolbiphenyl (**CBP**) has been used widely as a host for red-PHOLEDs, they usually require high driving voltages because the wide energy gap of **CBP** leads to large energy barriers for charge injection from adjacent carrier-transporting layers. In addition, **CBP** is inherently a *p*-type material; its hole mobility is at least one order of magnitude higher than its electron mobility.[17,18] Moreover, **CBP** exhibits a relatively low glass-transition temperature ($T_g$ = 62 °C)[19] and is prone to crystallization.[20–22] Its poor thermal and morphological stabilities may reduce **CBP**'s ability to bear joule heat during device operation.

In this study, we synthesized a host material, **SAF**, comprising electron-rich triphenylamine and electron-deficient 2,7-bis(phenylsulfonyl)fluorene units linked through the C9 position of the fluorene moiety. This molecular design endows **SAF** with several advantageous properties: (i) bipolarity, arising from the presence of the electron-accepting phenylsulfonyl groups appended to the triphenylamine/fluorene hybrid,[23–25] thereby facilitating both electron and hole injection and transport; (ii) a high triplet energy gap ($E_T$ = 2.71 eV), resulting from the individual building blocks being connected through a nonconjugated linkage (the sp$^3$-hybridized C9 atom of the fluorene unit), to effectively suppress reverse energy transfer from the guest emitter to the **SAF** host; and (iii) a sterically bulky and hindered structure imparting good thermal and morphological stabilities. As a result, we expected **SAF** to be an appropriate host for red-PHOLEDs. Indeed, an **SAF**-based red-PHOLED doped with 7 wt% tris(1-phenylisoquinolinolato-$C^2$,*N*)iridium(III) [Ir(piq)$_3$] exhibited a very low turn-on voltage (2.4 V) and high electroluminescence (EL) efficiencies of 15.8% and 22.0 lm W$^{-1}$, superior to those of the reference device based on the conventional material **CBP** (3.2 V, 8.5%, and 8.4 lm W$^{-1}$, respectively).

Recently, we reported an efficient bipolar host 2,7-bis(diphenylphosphoryl)-9-[4-(*N*,*N*-diphenylamino)phenyl]-9-phenylfluorene (POAPF) for a blue-PHOLED.[26] However, the relatively weak electron-withdrawing nature of diphenylphosphoryl segments in the POAPF molecule leads to an elevated lowest unoccupied molecular orbital (LUMO) level (−2.40 eV), which may impede electron injection from the electron-transporting layer. In addition, the mismatch of the LUMO energy level of POAPF with that of Ir(piq)$_3$ (−3.10 eV) would cause serious electron trapping at the dopant sites. Both of these influences will significantly increase the operating voltage of the red-PHOLED based on POAPF.

[a]*Department of Applied Chemistry, National Chiao Tung University, Hsinchu, 300 Taiwan. E-mail: shu@cc.nctu.edu.tw*
[b]*Institute of Chemistry, Academia Sinica, Taipei, Taiwan 11529, Republic of China*

 

## Results and discussion

### Synthesis and characterization

Scheme 1 illustrates the synthetic route followed for the preparation of the bipolar host **SAF**. The starting material, 2,7-dibromofluorenone, was treated with thiophenol in the presence of potassium carbonate in *N*,*N*-dimethylformamide (DMF) at 130 °C to afford the disulfide **1**, which was then reacted with the Grignard reagent of bromobenzene to give the corresponding alcohol **2**. Subsequent oxidation with 30% aqueous hydrogen peroxide yielded the disulfonyl intermediate **3**. The target compound **SAF** was obtained from the acid-promoted Friedel–Craft-type substitution of **3** with excess triphenylamine. We characterized the structure of **SAF** using $^{1}H$ and $^{13}C$ NMR spectroscopy, high-resolution mass spectrometry, and elemental analysis.

### Thermal properties

**SAF** exhibits very high thermal stability; thermogravimetric analysis (TGA) performed under a nitrogen atmosphere revealed that the decomposition temperature ($T_d$, corresponding to 5% weight loss) was 430 °C. The high value of $T_d$ of **SAF** implies that it is capable of enduring vacuum thermal sublimation, which meets one of the basic requirements of a host to be used in PHOLEDs. From differential scanning calorimetry (DSC) measurements, we observed a distinct glass transition temperature ($T_g$) at 127 °C—much higher than that of the conventional host material **CBP** ($T_g$ = 62 °C)[19]—and no exothermic peak resulting from crystallization at temperatures up to 280 °C. We attributed these superior thermal properties to the nonplanar, rigid structure of **SAF**, featuring a bulky triphenylamine group and two phenylsulfonyl units appended at the 9- and 2,7-positions of the fluorene ring, respectively. It is important for OLEDs to be constructed from materials having relatively high values of $T_g$ if they are to avoid degradation through morphological changes of the amorphous organic layer.[27–29] To further investigate the morphological stability of the emitting layer (EML) within the red-PHOLEDs, we used vacuum deposition to prepare **SAF** and **CBP** thin films (30 nm) doped with 7 wt% $Ir(piq)_3$ on silicon wafers and then measured their surface morphologies using atomic force microscopy (AFM) before and after annealing at 90 °C for 12 h under a nitrogen atmosphere. Fig. 1 reveals that the **SAF**-based thin film had a fairly stable surface morphology, which did not change upon annealing. The root mean square (RMS) roughness before and after annealing were 0.42 and 0.45 nm, respectively. On the other hand,

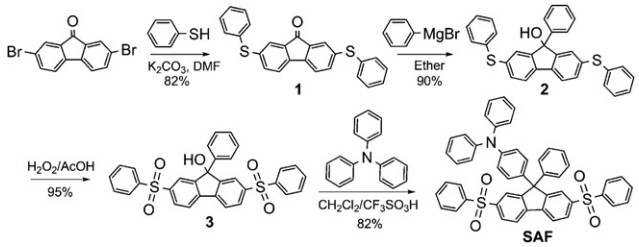


**Scheme 1** Synthetic route for **SAF**.

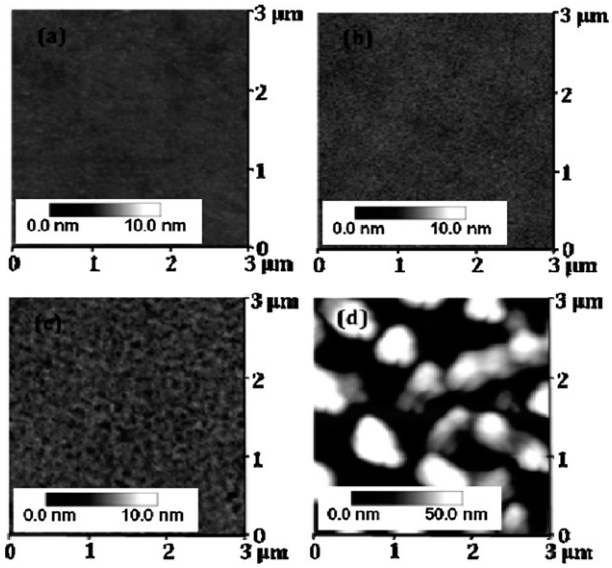


**Fig. 1** AFM images of 7 wt% $Ir(piq)_3$-doped films based on the hosts (a) **SAF** without annealing, (b) **SAF** with annealing, (c) **CBP** without annealing, and (d) **CBP** with annealing.

annealing the **CBP**-based film induced a degradation of the surface morphology, with large crystals appearing on the annealed film. The RMS roughness before and after the annealing of the **CBP**-based film were 0.57 and 18.6 nm, respectively. **SAF** maintained its morphological stability in the glassy state for long periods of heat exposure.

### Photophysical properties

Fig. 2a displays the UV-Vis absorption and photoluminescence (PL) spectra of **SAF** measured under different conditions; Table 1 summarizes the key spectral data. The absorption profiles of **SAF** in cyclohexane, toluene, and THF are nearly identical—*i.e.*, independent on solvent polarity—indicating that the Franck–Condon excited state is subject to a rather small dipolar change with respect to the ground state. In sharp contrast, the fluorescent maxima of **SAF** revealed a salient bathochromic shift: from

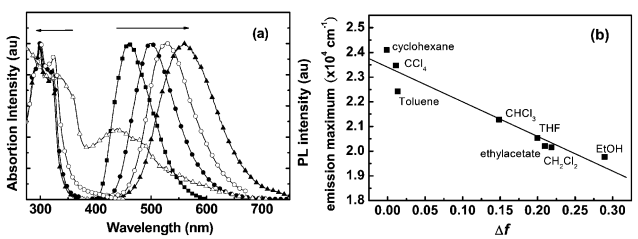


**Fig. 2** (a) Room-temperature absorption and PL spectra (excited at 335 nm) of **SAF** in cyclohexane (■), toluene (●), and THF (▲) solutions and as a solid film (○). The absorption spectrum of the $Ir(piq)_3$ film is also depicted (△). All films were formed on quartz substrates through thermal evaporation (30 nm). (b) Emission peak frequencies plotted as a function of the solvent polarities for **SAF** in various solutions. The solvent polarity parameter function $\Delta f$ is expressed using the formula $\Delta f = [(\varepsilon - 1)/(2\varepsilon + 1)] - [(n^2 - 1)/(2n^2 + 1)]$, where $\varepsilon$ is the static dielectric constant and $n$ is the optical refractivity index of the solvent.

**Table 1** Optical and thermal properties of **SAF**

| | $\lambda_{abs}$[a] [nm] | | | | $\lambda_{em,\ max}$ [nm] | | | | | |
|---|---|---|---|---|---|---|---|---|---|---|
| Host | *c*Hex | Tol | THF | Film | *c*Hex | Tol | THF | Film | $E_T$ [eV] | $T_g/T_d$ [°C] |
| **SAF** | 299, 321 | 299, 323 | 299, 323 | 301, 325 | 460 | 506 | 560 | 528 | 2.71 | 127/430 |

[a] Absorption wavelength, measured in cyclohexane (*c*Hex), toluene (Tol), and tetrahydrofuran (THF) solutions and in the thin film.

460 nm in nonpolar cyclohexane to 560 nm in highly polar THF. Furthermore, the excitation spectra of **SAF**, within experimental error, were effectively identical to the absorption spectra, indicating that the emissions result from a common Franck–Condon excited state. In addition, when we varied the concentration of **SAF** in each solution over the range $10^{-4}$ to $10^{-6}$ M, the absorption and emission profiles all exhibited concentration-independence. Thus, we can eliminate the possibility of the emission being caused by aggregates and/or excimers. We tentatively attribute the distinct solvatochromism in PL spectra of **SAF** to a mechanism involving rapid photoinduced electron transfer between the electron donor (triphenylamine) and the electron acceptor [2,7-bis(phenylsulfonyl)fluorene], resulting in a large change in the dipole moment in the excited state; a subsequent solvent relaxation process leads to the solvent polarity-dependent emission. When we plotted the emission peak frequencies of **SAF** in various organic solvents (from cyclohexane to ethanol) as a function of the solvent polarity (Fig. 2b), we obtained a linear relationship together with a slope as steep as $-14\,240$ $cm^{-1}$, consistent with our assignment of a charge-transfer emission. Similar results were reported and reviewed for other bipolar-type molecules.[30–32]

Moreover, there is an effective overlap between the PL spectrum of **SAF** and the absorption spectrum of the red-emitting phosphor $Ir(piq)_3$ (Fig. 2a). Thus, we anticipated that efficient Förster energy transfer of singlet excitons would occur from **SAF** to $Ir(piq)_3$. In the EL spectrum of the 7 wt% $Ir(piq)_3$–doped device (*vide infra*), we observe only the red emission from the triplet dopant, indicating the complete energy transfer from **SAF** to $Ir(piq)_3$. The absorption spectra (not shown) of the blue-emitting bis[(4,6-difluorophenyl)pyridinato-*N*,*C*$^{2'}$](picolinato)iridium(III) (FIrpic) and green-emitting *fac*-tris(2-phenylpyridinato)-iridium(III) [$Ir(ppy)_3$] overlap poorly with the emission spectrum of **SAF**, thereby prohibiting efficient energy transfer between the host and these phosphors. In addition, the nonconjugated linkage between the *n*- and *p*-type groups endows **SAF** with a high value of $E_T$ of 2.71 eV, estimated from the highest-energy 0–0 phosphorescent emission measured in frozen 2-methyltetrahydrofuran at 77 K. This value of $E_T$ is sufficiently high for **SAF** to undergo efficient exothermic energy transfer of triplet excitons to the red triplet emitter $Ir(piq)_3$ ($E_T = 2.0$ eV)[33] without reversing.

## Electrochemical properties

Fig. 3 displays the cyclic voltammograms of **SAF** and **CBP** in solutions containing ferrocene/ferrocenium ($Fc/Fc^+$) as the internal standard. Table 2 summarizes the redox onset potentials and calculated energy levels. During cathodic sweeping in DMF, both **SAF** and **CBP** exhibited reversible reduction waves, with

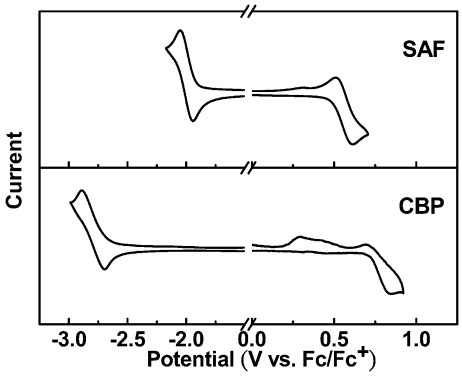


**Fig. 3** Cyclic voltammograms of **SAF** and **CBP**.

onset potentials at $-1.92$ and $-2.70$ V, respectively. The end-capping of the two electron-withdrawing phenylsulfonyl units at the fluorene group provided **SAF** with a less negative reduction potential relative to that of **CBP**. When performing anodic scans in $CH_2Cl_2$, **SAF** and **CBP** underwent oxidation processes with onset potentials of 0.49 and 0.72 V, originating from their electron-rich triphenylamine and carbazole segments, respectively. The oxidation of **SAF** occurred at a lower potential, indicating that the oxidation process was facilitated upon replacing the carbazole building block with a triphenylamine unit.[25] On the basis of the onset potentials for oxidation and reduction, we estimated the highest occupied/lowest unoccupied molecular orbital (HOMO/LUMO) levels of **SAF** and **CBP** with regard to the energy level of ferrocene (4.8 eV below vacuum). Fig. 4 displays the relative HOMO/LUMO energy levels of the materials used to prepare the devices. **SAF** possesses lower LUMO ($-2.88$ eV) and shallower HOMO ($-5.29$ eV) levels than those of **CBP** ($-2.10$ and $-5.52$ eV, respectively), revealing its superior ability to inject electrons and holes.

## Electroluminescence properties

To evaluate the bipolar characteristics of **SAF**, we prepared hole-only devices having the architecture indium tin oxide (ITO)/*N*,*N*′-diphenyl-*N*,*N*′-bis(3-methylphenyl)-(1,1′-biphenyl)-4,4′-diamine (TPD, 30 nm)/host (30 nm)/TPD (30 nm)/Al (100 nm) and electron-only devices having the configuration

**Table 2** Electrochemical data for the hosts

| Host | $E_{ox}^{onset}$ [V] | $E_{red}^{onset}$ [V] | HOMO [eV] | LUMO [eV] |
|---|---|---|---|---|
| **SAF** | 0.49 | $-1.92$ | $-5.29$ | $-2.88$ |
| **CBP** | 0.72 | $-2.70$ | $-5.52$ | $-2.10$ |

 

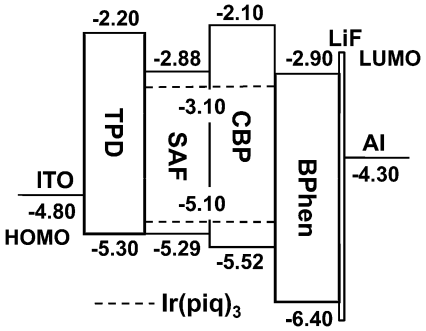


**Fig. 4** Relative HOMO/LUMO energy levels of the materials used for the EL devices.

ITO/4,7-diphenyl-1,10-phenanthroline (BPhen, 30 nm)/host (30 nm)/BPhen (30 nm)/LiF (15 Å)/Al (100 nm). Here, the host materials were **SAF** and the conventional host **CBP**. In the case of the hole-only devices, because of the large energy injection barrier between TPD (LUMO = −2.20 eV) and Al (−4.30 eV), most electrons were restrained from injection into the organic layer. Only holes could be injected from the anode to the organic layers; therefore, the measured current density–voltage (*I–V*) characteristics were dominated by holes. On the other hand, in the electron-only devices, the BPhen layer possessed a large HOMO energy level (–6.40 eV) and, therefore, it behaved as a hole-blocker to inhibit the injection of holes from the ITO anode (−4.80 eV) to the organic layer. Thus, the measured *I–V* curves mostly reflect the injected electrons. Fig. 5 reveals that both the **SAF**-based hole- and electron-only devices exhibited lower turn-on voltages and higher current densities than did the corresponding **CBP**-based devices under the same bias. We attribute the reduced driving voltages in the **SAF**-based devices to the decreased barrier heights for hole and electron injection from the charge transport layers to **SAF**. From these studies of carrier-only devices, we anticipated that the use of **SAF** as a host in PHOLEDs would provide suitable energy levels to facilitate carrier injection.

Furthermore, we measured the carrier mobility in the **SAF** film using time-of-flight (TOF) transient photocurrent techniques. The bipolar charge-transporting capability of **SAF** was evidenced by the similar values for the electron ($3.4 \times 10^{-5}$ cm$^2$ V$^{-1}$ s$^{-1}$) and hole mobilities ($3.5 \times 10^{-5}$ cm$^2$ V$^{-1}$ s$^{-1}$) under an electric field of $4.1 \times 10^{-5}$ V cm$^{-1}$. In contrast, the electron and hole mobilities of **CBP** were on the orders of $10^{-4}$ and $10^{-3}$ cm$^2$ V$^{-1}$ s$^{-1}$, respectively,[17,18] indicating relatively unbalanced charge fluxes in the **CBP**-based EML. Although the electron and hole mobilities of **SAF** were more than one order of magnitude lower than those of **CBP**, the measured current densities of the **SAF**-based carrier-only devices (Fig. 5) were higher than those of its **CBP** counterparts at the same driving voltages. This behavior may suggest that the current fluxes in **CBP** carrier-only devices are significantly limited by the potential barriers presented at the carrier-transporting layer–**CBP** interfaces, with the device currents being dictated primarily by the efficiencies of carrier injection (*i.e.*, energy barriers), rather than the carrier mobility of the host material.[34,35]

Subsequently, we doped the bipolar host material **SAF** with a commercially available triplet phosphor, Ir(piq)$_3$, to realize a highly efficient red-PHOLED. The device was fabricated in the configuration ITO/TPD (30 nm)/EML (30 nm)/BPhen (30 nm)/LiF (15Å)/Al (100 nm). Here, "EML" refers to a layer of **SAF** doped with 7 wt% Ir(piq)$_3$; TPD and BPhen functioned not only as hole- and electron-transporting layers but also as the carrier-blockers for effective emission.[36,37] For comparison, we also fabricated the reference device incorporating the conventional host material **CBP**. Fig. 6 displays the current density–voltage–luminance (*I–V–L*) characteristics of these red-PHOLEDs. The **SAF**-based device exhibited significantly lower operating voltages than its **CBP** counterpart under the same current density, presumably because of the smaller energy barriers when using **SAF** as the host material, as demonstrated in the carrier-only devices (*vide supra*). As a result, the **SAF** device had a relatively low turn-on voltage of 2.4 V (corresponding to 1 cd m$^2$). In addition, the **SAF**-based device exhibited a much better peak external quantum efficiency (EQE, 15.8% at 21.9 cd m$^{-2}$) than its **CBP** counterpart (8.5% at 93.0 cd m$^{-2}$). We attribute this behavior to the relatively balanced bipolar transport of **SAF** (*vide supra*), thereby increasing the opportunity for carrier recombination, and the higher value of $E_T$ of **SAF** (2.71 eV) relative to that of **CBP** (2.56 eV), thereby effectively suppressing reverse energy transfer from the triplet dopant to the host.[20] The combination of a low operating voltage and a high EQE afforded our **SAF**-based device with an extremely high power efficiency (PE) of 22.0 lm W$^{-1}$. Even at a practical brightness of 1000 cd m$^{-2}$, the operating voltage was merely 3.6 V and the

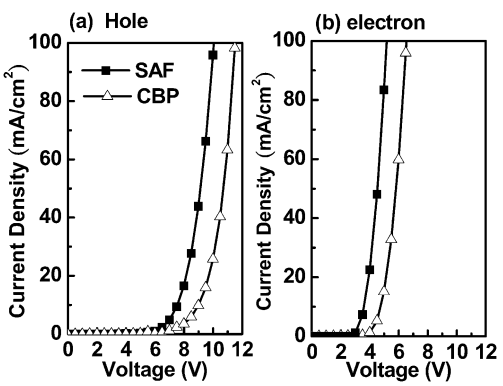


**Fig. 5** *I–V* characteristics of (a) hole- and (b) electron-only devices.

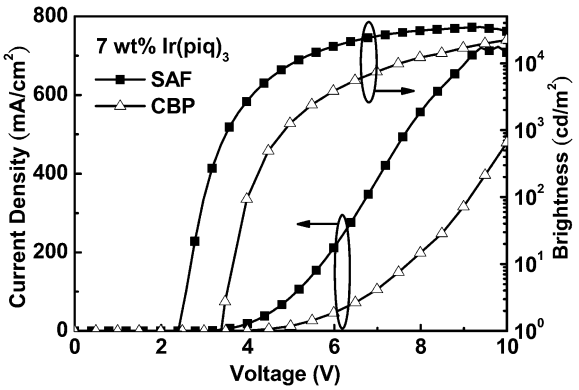


**Fig. 6** *I–V–L* characteristics of Ir(piq)$_3$–doped devices.

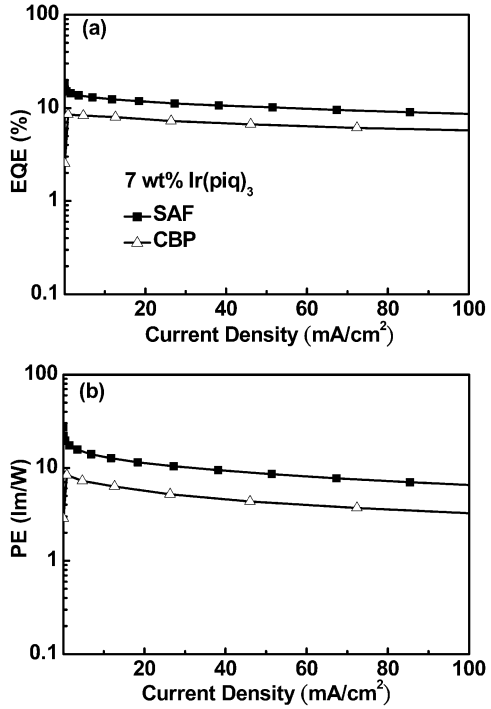


**Fig. 7** (a) EQE and (b) PE of the $Ir(piq)_3$-doped devices plotted with respect to the current density.

**Table 3** Electroluminescence data for the devices

| Host | SAF | CBP |
|---|---|---|
| $V$ [a] [V] | 2.4/3.6 | 3.2/4.9 |
| EQE [b] [%] | 15.8/13.1 | 8.5/7.3 |
| PE [b] [lm $W^{-1}$] | 22.0/14.4 | 8.4/5.7 |
| LE [b] [cd $A^{-1}$] | 19.6/16.2 | 10.6/8.8 |
| CIE [c] [$x$, $y$] | 0.67,0.33 | 0.67,0.33 |

[a] Measured operating voltages, presented in the order of the values at 1 and 1000 cd $m^{-2}$. [b] Measured values, presented in the order of the maximum value and the value at 1000 cd $m^{-2}$. [c] Measured at 7 V.

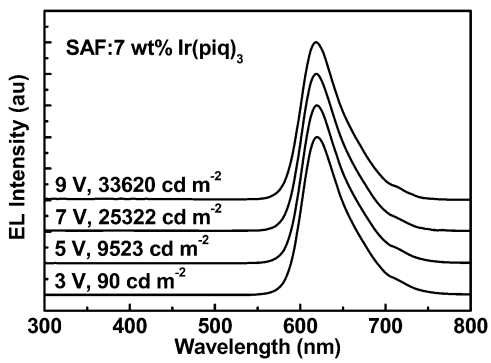


**Fig. 8** EL spectra of the **SAF**-based device recorded under various operating voltages.

efficiencies remained high (13.1%, 14.4 lm $W^{-1}$). Fig. 7 presents plots of the EQE and PE with respect to the current density for these red-electrophosphorescent devices; Table 3 lists their key characteristics. Moreover, the EL spectra of the **SAF**-based device exhibited almost the same profiles, with the maximum signal intensity at 622 nm, over the entire range of operating voltages (Fig. 8), with Commission Internationale de L'Eclairage (CIE) coordinates at the standard red (0.67, 0.33) demanded by the NTSC. The spectra were assigned to the emission from $Ir(piq)_3$, without any other emission originating from the adjacent organic layer, indicating the excellent confinement of carriers within the EML.

## Conclusion

We have synthesized a novel bipolar host (**SAF**) for the fabrication of highly efficient $Ir(piq)_3$-based red-PHOLEDs. **SAF** was constructed by linking an electron-rich triphenylamine group to an electron-deficient bis(phenylsulfonyl)-substituted fluorene through the C9 atom of its fluorene unit. This geometry afforded **SAF** with a rather bulky and nonplanar structure and, hence, high thermal and morphological stabilities. In addition, the introduction of a nonconjugated linkage resulted in a high value of $E_T$ (2.71 eV), which effectively prevented reverse energy transfer from the triplet emitter to the **SAF** host. More importantly, the favorable bipolar characteristics of **SAF** facilitated both hole and electron injection from adjacent carrier-transporting layers and balanced charge fluxes within the EML. Consequently, the 7 wt% $Ir(piq)_3$-doped **SAF** device exhibited significantly improved EL efficiencies (15.8% and 22.0 lm $W^{-1}$) relative to those of the reference device incorporating the conventional host **CBP** (8.5%, 8.4 lm $W^{-1}$).

## Experimental section

### Characterization

$^1H$ and $^{13}C$ NMR spectra were recorded using Varian UNITY INOVA 500 MHz and Varian UNITY 300 MHz spectrometers. Mass spectra and high-resolution mass spectra (HRMS) were obtained using JEOL JMS-HX 110 and Finnigan Thermo Quest MAT 95XL mass spectrometers. Differential scanning calorimetry (DSC) was performed using a SEIKO EXSTAR 6000DSC unit operated at heating and cooling rates of 10 and 50 °C $min^{-1}$, respectively. The glass transition temperature ($T_g$) was determined from the second heating scan. Thermogravimetric analysis (TGA) was undertaken using a DuPont TGA 2950 instrument. The thermal stability of the samples under a nitrogen atmosphere was determined by measuring their weight losses while heating at a rate of 20 °C $min^{-1}$. Atomic force microscopy (AFM) measurements were performed in the tapping mode under ambient conditions using a Digital Nanoscope IIIa instrument. UV-Vis spectra were measured using an HP 8453 diode array spectrophotometer. PL spectra were obtained using a Hitachi F4500 luminescence spectrometer. The low-temperature phosphorescence spectra were obtained using a composite spectrometer containing a monochromator (Jobin Yvon, Triax 190) coupled with a liquid nitrogen-cooled charge-coupled device (CCD) detector (Jobin Yvon, CCD-1024 × 256-open-1LS). Cyclic voltammetry (CV) measurements were performed using a BAS 100 B/W electrochemical analyzer operated at a scan rate of 100 mV $s^{-1}$. The potentials were measured against an $Ag/Ag^+$ (0.01 M $AgNO_3$) reference electrode using ferrocene/ferrocenium ($Fc/Fc^+$) as the internal standard.

 

### Carrier mobility

The carrier mobility was measured using time-of-flight transient photocurrent techniques at ambient temperature. The sample was fabricated in the configuration glass/ITO (100 nm)/**SAF** (1 μm)/Ag (20 nm). The **SAF** layer was deposited at a constant rate of 0.15 nm $s^{-1}$. During the film deposition of the devices, the pressure of the chamber was maintained below $2 \times 10^{-6}$ torr to minimize defects and the evaporation rates of the organic materials were controlled using respective quartz-crystal monitors. The thickness of the organic layer was measured using a surface profiler (Dektak 150; Veeco). The frequency-doubled output of a 5 ns-pulsed dye laser at 295 nm was chosen to maximize the optical absorption of the organic layer. The laser beam was directed through the samples from the Ag side to create photoexcited carriers. The excitation power density was set at *ca.* 1.6 W $cm^{-2}$ to avoid space-charge effects. The instrumental response time was maintained much shorter than the transit time. The transient photocurrent was recorded by measuring the voltage across a 50 Ω resistor using a 1 GHz digital oscilloscope (LC574 AM, LeCroy). The transit time, $t_T$, was taken from the intersection of two clear straight lines in the double-logarithmic plot of the transient photocurrent profile. The carrier mobility $\mu$ was given by $\mu = D/t_T E$, where $D$ is the thickness of the organic layer and $E$ is the applied electric field. The detection of the transient photocurrent signal was performed using a process similar to one described previously.[38]

### Fabrication of PHOLEDs

The EL devices were fabricated through vacuum deposition of the materials at $10^{-6}$ torr onto ITO glass having a sheet resistance of 25 Ω $square^{-1}$. All of the organic layers were deposited at a rate of 1.0 Å $s^{-1}$. The cathode was completed through thermal deposition of LiF at a deposition rate of 0.1 Å $s^{-1}$; it was then capped with Al metal through thermal evaporation at a rate of 4.0 Å $s^{-1}$. The current density–voltage and brightness–voltage relationships of the devices were measured using a Keithley 2400 source meter and a Newport 1835C optical meter equipped with an 818ST silicon photodiode. The EL spectrum was obtained using a Hitachi F4500 luminescence spectrometer.

### 2,7-Bis(phenylthio)fluorenone (1)

2,7-Dibromofluorenone (3.06 g, 9.05 mmol) was added to a mixture of $K_2CO_3$ (2.76 g, 20.0 mmol) and *N*,*N*-dimethylformamide (150 mL). Thiophenol (1.95 mL, 19.0 mmol) was added with stirring and then the solution was heated at 130 °C for 6 h. The reaction mixture was cooled to room temperature and poured into water (600 mL). The orange precipitate was collected by filtration, washed with water, and dried under vacuum. The solid was recrystallized (ethyl acetate/*n*-hexane) to afford orange needles (2.94 g, 82%). $^1$H NMR (300 MHz, $CDCl_3$, δ): 7.51 (s, 2H), 7.43–7.28 (m, 14H); $^{13}$C NMR (75 MHz, $CDCl_3$, δ): 192.83, 142.51, 138.85, 136.19, 135.19, 134.32, 132.44, 129.85, 129.31, 126.20, 121.12; MS (EI, *m*/*z*): 396 [$M^+$].

### 2,7-Bis(phenylthio)-9-phenyl-9-fluorenol (2)

The Grignard reagent was prepared from Mg powder (0.37 g, 15.2 mmol) and bromobenzene (1.71 mL, 16.2 mmol) in ether (150 mL). **1** (5.08 g, 12.8 mmol) was added into the cooled Grignard solution. The reaction mixture was stirred for 8 h at room temperature and then it was quenched with saturated $NH_4Cl$ aqueous solution (150 mL) and extracted with ethyl acetate (3 × 100 mL). The collected organic phase was dried ($MgSO_4$) and concentrated under reduced pressure. The residue was washed with hot *n*-hexane (150 mL) to give a pale-orange solid (5.50 g, 90%). $^1$H NMR (300 MHz, $CDCl_3$, δ): 7.58 (d, $J$ = 7.8 Hz, 2H), 7.38–7.24 (m, 19H), 2.50 (s, 1H); $^{13}$C NMR (75 MHz, $CDCl_3$, δ): 151.62, 142.64, 138.28, 136.71, 135.84, 132.17, 131.30, 129.58, 128.69, 127.87, 127.76, 127.53, 125.62, 121.10, 83.74; MS (EI, *m*/*z*): 474 [$M^+$].

### 2,7-Bis(phenylsulfonyl)-9-phenyl-9-fluorenol (3)

30% Aqueous hydrogen peroxide (30 mL) was added to a solution of **2** (2.58 g, 5.43 mmol) in acetic acid (70 mL). The reaction mixture was stirred at 80 °C for 24 h and then it was cooled to room temperature, saturated with NaCl (*ca.* 15 g), and extracted with $CH_2Cl_2$ (4 × 70 mL). The combined organic phases were dried ($MgSO_4$) and the solvents evaporated under reduced pressure to provide a pale-yellow residue, which was recrystallized from a mixture of $CHCl_3$ and *n*-hexane to give a white solid (2.76 g, 95%). $^1$H NMR (300 MHz, $CDCl_3$, δ): 7.94–7.90 (m, 5H), 7.87–7.84 (m, 5H), 7.77–7.73 (m, 3H), 7.56–7.42 (m, 8H); $^{13}$C NMR (75 MHz, $CDCl_3$, δ): 152.56, 142.98, 142.55, 141.38, 140.72, 133.61, 129.61, 128.97, 128.47, 127.86, 125.36, 124.64, 122.06, 83.60; MS (EI, *m*/*z*): 538 [$M^+$].

### 2,7-Bis(phenylsulfonyl)-9-(4-*N*,*N*-diphenylamino)phenyl-9-phenylfluorene (SAF)

$CF_3SO_3H$ (1.10 mL, 12.5 mmol) was added dropwise to a solution of triphenylamine (4.85 g, 19.8 mmol) and **3** (5.26 g, 9.78 mmol) in $CH_2Cl_2$ (200 mL). The mixture was stirred for 30 min at room temperature and then quenched with saturated aqueous $NaHCO_3$ solution (100 mL). The organic phase was washed twice with water (100 mL) and then it was dried ($MgSO_4$). After evaporation of the volatiles, the residue was purified through column chromatography ($SiO_2$; $CH_2Cl_2$/hexane, 1:5) to yield **SAF** as a yellow solid (6.14 g, 82%). $^1$H NMR (300 MHz, [$D_8$]THF, δ): 8.11 (s, 2H), 8.07 (d, $J$ = 8.1 Hz, 2H), 7.98 (dd, $J$ = 8.1, 1.5 Hz, 2H), 7.89 (d, $J$ = 6.9 Hz, 4H), 7.55–7.43 (m, 6H), 7.25–7.14 (m, 9H), 7.04–6.98 (m, 8H), 6.88 (d, $J$ = 8.7 Hz, 2H); $^{13}$C NMR (75 MHz, [$D_8$]THF, δ): 153.48, 147.79, 147.33, 144.12, 143.05, 142.99, 142.69, 137.26, 133.08, 129.34, 128.72, 128.69, 127.89, 127.86, 127.69, 127.39, 125.89, 124.62, 123.18, 123.11, 122.35, 65.67; HRMS (FAB, *m*/*z*): calcd for $C_{49}H_{36}NO_4S_2$ [M + H]$^+$, 766.2086; found, 766.2073; Anal. Calcd for $C_{49}H_{35}NO_4S_2$: C 76.84, H 4.61, N, 1.83; found: C 76.46, H 4.70, N 1.72.

## Acknowledgements

We thank the National Science Council for funding and Professor C.-H. Cheng for his support during the preparation and characterization of the PHOLEDs.

## References


1 M. A. Baldo, D. F. O'Brien, Y. You, A. Shoustikov, S. Sibley, M. E. Thompson and S. R. Forrest, *Nature*, 1998, **395**, 151.
2 J. Brooks, Y. Babayan, S. Lamansky, P. I. Djurovich, I. Tsyba, R. Bau and M. E. Thompson, *Inorg. Chem.*, 2002, **41**, 3055.
3 S. Y. Chang, J. Kavitha, S. W. Li, C. S. Hsu, Y. Chi, Y. S. Yeh, P. T. Chou, G. H. Lee, A. J. Carty, Y. T. Tao and C. H. Chien, *Inorg. Chem.*, 2006, **45**, 137.
4 S. Lamansky, P. Djurovich, D. Murphy, F. Abdel-Razzaq, H. E. Lee, C. Adachi, P. E. Burrows, S. R. Forrest and M. E. Thompson, *J. Am. Chem. Soc.*, 2001, **123**, 4304.
5 F. C. Chen, Y. Yang, M. E. Thompson and J. Kido, *Appl. Phys. Lett.*, 2002, **80**, 2308.
6 B. Tong, Q. Mei, S. Wang, Y. Fang, Y. Meng and B. Wang, *J. Mater. Chem.*, 2008, **18**, 1636.
7 B. Carlson, G. D. Phelan, W. Kaminsky, L. Dalton, X. Jiang, S. Liu and A. K. Y. Jen, *J. Am. Chem. Soc.*, 2002, **124**, 14162.
8 S. Bernhard, X. Gao, G. G. Malliaras and H. D. Abruña, *Adv. Mater.*, 2002, **14**, 433.
9 Y. L. Tung, S. W. Lee, Y. Chi, Y. T. Tao, C. H. Chien, Y. M. Cheng, P. T. Chou, S. M. Peng and C. S. Liu, *J. Mater. Chem.*, 2005, **15**, 460.
10 H. Rudmann, S. Shimada and M. F. Rubner, *J. Am. Chem. Soc.*, 2002, **124**, 4918.
11 M. A. Baldo, C. Adachi and S. R. Forrest, *Phys. Rev. B: Condens. Matter Mater. Phys.*, 2000, **62**, 10967.
12 M. A. Baldo, M. E. Thompson and S. R. Forrest, *Nature*, 2000, **403**, 750.
13 T. Fuhrmann and J. Salbeck, *MRS Bull.*, 2003, **28**, 354.
14 B. W. D'Andrade and S. R. Forrest, *Adv. Mater.*, 2004, **16**, 1585.
15 H. Kanno, R. J. Holmes, Y. Sun, S. Kena-Cohen and S. R. Forrest, *Adv. Mater.*, 2006, **18**, 339.
16 Y. Tao, Q. Wang, Y. Shang, C. Yang, L. Ao, J. Qin, D. Ma and Z. Shuai, *Chem. Commun.*, 2009, 77.
17 J. W. Kang, S. H. Lee, H. D. Park, W. I. Jeong, K. M. Yoo, Y. S. Park and J. J. Kim, *Appl. Phys. Lett.*, 2007, **90**, 223508.
18 H.-I. Baek and C. H. Lee, *J. Appl. Phys.*, 2008, **103**, 054510.
19 M. H. Tsai, Y. H. Hong, C. H. Chang, H. C. Su, C. C. Wu, A. Matoliukstyte, J. Simokaitiene, S. Grigalevicius, J. V. Grazulevicius and C. P. Hsu, *Adv. Mater.*, 2007, **19**, 862.
20 G. Zhou, W. Y. Wong, B. Yao, Z. Xie and L. Wang, *Angew. Chem., Int. Ed.*, 2007, **46**, 1149.
21 C. L. Ho, W. Y. Wong, Z. Q. Gao, C. H. Chen, K. W. Cheah, B. Yao, Z. Xie, Q. Wang, D. Ma, L. Wang, X. M. Yu, H. S. Kwok and Z. Lin, *Adv. Funct. Mater.*, 2008, **18**, 319.
22 Y. Tao, Q. Wang, C. Yang, Q. Wang, Z. Zhang, T. Zou, J. Qin and D. Ma, *Angew. Chem., Int. Ed.*, 2008, **47**, 8104.
23 I. I. Perepichka, I. F. Perepichka, M. R. Bryce and L.-O. Pålsson, *Chem. Commun.*, 2005, 3397.
24 T. H. Huang, J. T. Lin, L. Y. Chen, Y. T. Lin and C. C. Wu, *Adv. Mater.*, 2006, **18**, 602.
25 P. J. Low, M. A. J. Paterson, D. S. Yufit, J. A. K. Howard, J. C. Cherryman, D. R. Tackley, R. Brook and B. Brown, *J. Mater. Chem.*, 2005, **15**, 2304.
26 F. M. Hsu, C. H. Chien, C. F. Shu, C. H. Lai, C. C. Hsieh, K. W. Wang and P. T. Chou, *Adv. Funct. Mater.*, 2009, **19**, 2834.
27 E. Han, L. Do, Y. Niidome and M. Fujihira, *Chem. Lett.*, 1994, 969.
28 S. Tokito and Y. Taga, *Appl. Phys. Lett.*, 1995, **66**, 673.
29 S. Liu, F. He, H. Wang, H. Xu, C. Wang, F. Li and Y. Ma, *J. Mater. Chem.*, 2008, **18**, 4802.
30 Y. Y. Chien, K. T. Wong, P. T. Chou and Y. M. Cheng, *Chem. Commun.*, 2002, 2874.
31 K. T. Wong, S. Y. Ku, Y. M. Cheng, X. Y. Lin, Y. Y. Hung, S. C. Pu, P. T. Chou, G. H. Lee and S. M. Peng, *J. Org. Chem.*, 2006, **71**, 456.
32 Z. R. Grabowski, K. Rotkiewicz and W. Rettig, *Chem. Rev.*, 2003, **103**, 3899.
33 T. Tsuzuki and S. Tokito, *Adv. Mater.*, 2007, **19**, 276.
34 S. W. Tsang, Z. H. Lu and Y. Tao, *Appl. Phys. Lett.*, 2007, **90**, 132115.
35 C. C. Chi, C. L. Chiang, S. W. Liu, H. Yueh, C. T. Chen and C. T. Chen, *J. Mater. Chem.*, 2009, **19**, 5561.
36 M. Yoshida, A. Fujii, Y. Ohmori and K. Yoshino, *Appl. Phys. Lett.*, 1996, **69**, 734.
37 J. H. Seo, J. H. Seo, J. H. Park, Y. K. Kim, J. H. Kim, G. W. Hyung, K. H. Lee and S. S. Yoon, *Appl. Phys. Lett.*, 2007, **90**, 203507.
38 S. W. Liu, J. H. Lee, C. C. Lee, C. T. Chen and J. K. Wang, *Appl. Phys. Lett.*, 2007, **91**, 142106.


 